第 43 卷 第 19 期/2023 年 10 月/光学学报 研究论文

光学学报

基于聚二甲基硅氧烷增敏的级联双腔温度传感器

杨玉强[1,2,4]，高佳乐[1,4]，牟小光[3*]，王骥[2,4**]，杨文虎[1,4]，李依潼[2,4]，王楚虹[4]

[1]广东海洋大学深圳研究院，广东 深圳 518120；

[2]广东海洋大学广东省船舶智能与安全工程技术研究中心，广东 湛江 524088；

[3]广东海洋大学机械工程学院，广东 湛江 524088；

[4]广东海洋大学智慧海洋传感网及其装备工程技术研究中心，广东 湛江 524088

摘要 提出并制备了一种基于聚二甲基硅氧烷(PDMS)增敏的级联双腔温度传感器，该传感器由PDMS腔和空气腔级联而成，且级联双腔的光程相近，从而干涉谱产生游标效应。此外，空气腔的两端均为PDMS，当温度增加时，空气腔两端的PDMS因膨胀同时挤压空气腔，大幅提高了空气腔的温度响应。在PDMS膨胀和游标效应的双重作用下，该传感器具有非常高的温度灵敏度。实验结果表明，在40～42 ℃范围内，传感器的温度灵敏度约为−20.55 nm /℃，相比单个PDMS腔提高了37倍。该传感器具有结构紧凑、灵敏度高、稳定性好等优点，具有很好的应用前景。

关键词 光纤光学与光通信；光纤传感器；法布里-珀罗干涉仪；游标效应；聚二甲基硅氧烷

中图分类号 O436 **文献标志码** A **DOI**：10.3788/AOS230442

1 引 言

温度是科学研究和工业生产中最基本、最重要的物理量，温度的测量和控制非常重要，因此，实现高精度温度测量一直是研究者追寻的目标[1-2]。与传统电学温度传感器相比，光纤温度传感器具有耐腐蚀、安全性好、抗电磁干扰等优点[3-4]，特别适合应用于高温、高压、易燃、易爆、强电磁场干扰等电信号测量受限的特殊环境。在众多光纤温度传感器中，光纤法布里-珀罗干涉仪(FPI)传感器还具有体积小、结构紧凑、便于集成的优点，受到了国内外学者的广泛关注[5-6]。然而，由于石英光纤的热膨胀和热光系数较低，导致全光纤FPI温度传感器的灵敏度仅约为84.6 pm/℃[7]。

提高光纤温度传感器灵敏度的一种常用方法是将热敏材料与光纤相结合，实验中经常使用的热敏材料是聚二甲基硅氧烷(PDMS)。PDMS是一种由弹性聚合物(Sylgard184-A)和硬化剂(Sylgard184-B)混合而成的温度敏感材料，最初为液态，在温度作用下将逐渐变为固态。PDMS不仅具有优异的热膨胀特性和热光特性，而且具有良好的粘接性、耐热性、耐寒性、防水性及化学惰性，因此，非常适合与光纤相结合制备性能优良的温度传感器。2016年，Hernández-Romano等[8]将PDMS涂覆在单模光纤顶端，成功制备了基于PDMS腔的FPI温度传感器，该温度传感器灵敏度为0.13 nm/℃；2018年，Zhao等[9]将PDMS注入一端与单模光纤熔接的空芯光纤内，成功制备了基于空气腔的FPI温度传感器，借助PDMS的高热膨胀特性，温度灵敏度达到了2.7 nm/℃；He等[10]将PDMS涂覆在无芯光纤上制备了一种基于马赫-曾德尔干涉仪(MZI)的温度传感器，该传感器的温度灵敏度为0.44 nm/℃。借助PDMS优良的温度特性，上述光纤温度传感器的灵敏度均有不同程度的提高。提高光纤干涉仪灵敏度的另一种有效方法是光学游标效应[11-15]。游标效应最初应用于提高长度测量的分辨率，如游标卡尺，其工作原理在于巧妙利用主尺与游标的微小比例尺差异。而光学游标效应的原理与游标卡尺类似，由两自由光谱范围(FSR)接近的干涉仪组成，两个干涉仪的作用分别与游标卡尺的“主尺”和“游标”的作用相似，利用两干涉仪FSR的微小差异实现灵敏度放大。目前，基于光学游标效应的干涉仪主要分为两FPI组合[16-17]、两MZI组合[18]、两Sagnac干涉仪(FSI)组合[19]，以及不同类干涉仪混合组合[20-21]，控制两个干涉仪的FSR使之相近但不相等，从而产生游标效应，使传感器的灵敏度提高几倍甚至几十倍。实验结果均表明，游标效应是提高光纤干涉仪测量灵敏度的一种有效方法。近年

收稿日期：2023-01-04；**修回日期**：2023-02-24；**录用日期**：2023-04-13；**网络首发日期**：2023-05-08

基金项目：广东省自然科学基金面上项目(2023A1515011212)、深圳市基础研究面上项目(JCYJ20210324122813036)、广东省普通高校重点领域专项(2021ZDZX1015)

通信作者：*xd_gdou@sina.com；**13902576499@163.com

来，为了进一步提高光纤干涉仪的灵敏度，研究者将光学游标效应与PDMS有机结合在一起。2019年，Mao等[22]将全光纤空气腔与PDMS增敏的空气腔并联，使其产生游标效应，该传感器温度灵敏度达到了17.758 nm/℃；2021年，Fu等[23]制备了基于空气腔与PDMS腔级联的温度传感器，该传感器灵敏度为3.89 nm/℃；2022年，本文课题组[24]将分别在光纤径向和横向热膨胀PDMS腔双腔并联，借助增敏性游标效应，该传感器温度灵敏度达到了−14.6 nm/℃。

本文提出并制备了一种基于PDMS增敏的级联双腔温度传感器，该传感器由PDMS腔和空气腔级联构成，且级联双腔的光程相近，从而干涉谱产生游标效应。此外，空气腔的两端均为PDMS，当温度增加时，空气腔两端的PDMS因膨胀同时挤压空气腔，大幅提高了空气腔的温度响应。在PDMS和游标效应的双重作用下，该传感器具有非常高的温度灵敏度。实验结果表明，在40～42 ℃范围内，传感器温度灵敏度约为−20.55 nm/℃。

2　传感器结构与工作原理

本文提出的光纤温度传感器结构如图1所示，该传感器由PDMS腔和空气腔级联而成。单模光纤（SMF）与一段空芯光纤（HCF）熔接，HCF内填充PDMS，构成PDMS腔；PDMS腔被封装在一端填充PDMS的石英管（tube）内，两端PDMS之间为空气，构成空气（air）腔。由于折射率不匹配，传感器内存在三个反射面M1、M2和M3，分别为SMF/PDMS、PDMS/air和air/PDMS截面。M1和M2之间为PDMS腔，腔长为L_1；M2和M3之间构成空气腔，腔长为L_2。

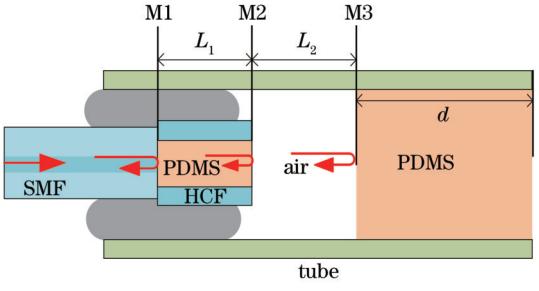

图1　提出传感器的结构示意图

Fig. 1　Schematic diagram of proposed sensor

由于反射面M1、M2和M3的反射率都非常低，因此，PDMS腔和空气腔的反射谱为典型的双光束干涉，可分别表示为

$$I_{\mathrm{PDMS}}=I_1+I_2-2\sqrt{I_1I_2}\cos\left(\frac{4\pi n_1L_1}{\lambda}\right),\tag{1}$$

$$I_{\mathrm{air}}=I_2+I_3-2\sqrt{I_2I_3}\cos\left(\frac{4\pi n_2L_2}{\lambda}\right),\tag{2}$$

式中：I_1、I_2和I_3分别为由M1、M2和M3反射回SMF的光强；$n_1\approx1.41$和$n_2\approx1.00$分别为PDMS和空气的折射率。PDMS腔和空气腔的温度灵敏度分别为

$$S_{\mathrm{PDMS}}=\lambda_{\mathrm{s}}\left(\frac{1}{L_1}\frac{dL_1}{dT}+\frac{1}{n_1}\frac{dn_1}{dT}\right)=\lambda_{\mathrm{s}}\left(\alpha+\frac{\beta}{n_1}\right),\tag{3}$$

$$S_{\mathrm{air}}=\lambda_{\mathrm{s}}\left(\frac{1}{L_2}\frac{dL_2}{dT}+\frac{1}{n_2}\frac{dn_2}{dT}\right)=\lambda_{\mathrm{s}}\left[\alpha(L_1+d)\right],\tag{4}$$

式中：$\alpha\approx9.6\times10^{-4}$/℃和$\beta\approx-5\times10^{-4}$/℃分别为PDMS的热膨胀系数和热光系数；$d$为石英管内填充的PDMS的长度；$\lambda_{\mathrm{s}}$为干涉谱峰值波长。当PDMS腔的FSR（$R_{\mathrm{PDMS}}=\lambda^2/2n_1L_1$）与空气腔的FSR（$R_{\mathrm{air}}=\lambda^2/2n_2L_2$）近似相等时，PDMS腔和空气腔之间将产生游标效应，形成干涉谱包络，该干涉谱包络[25]可表示为

$$I_{\mathrm{envelope}}=D+2m\cos\left[\frac{4\pi(n_1L_1-n_2L_2)}{\lambda}\right],\tag{5}$$

式中：D为干涉谱包络的直流部分；m为干涉谱包络交流部分振幅。当$n_1L_1>n_2L_2$时，干涉谱包络的FSR为$R_{\mathrm{en}}=\lambda^2/2(n_1L_1-n_2L_2)=R_{\mathrm{air}}\times R_{\mathrm{PDMS}}/(R_{\mathrm{air}}-R_{\mathrm{PDMS}})$；当$n_1L_1<n_2L_2$时，干涉谱包络的FSR为$R_{\mathrm{en}}=\lambda^2/2(n_2L_2-n_1L_1)=R_{\mathrm{air}}\times R_{\mathrm{PDMS}}/(R_{\mathrm{PDMS}}-R_{\mathrm{air}})$。当温度变化时，干涉谱包络平移量远远大于单个PDMS腔和单个空气腔，其灵敏度可表示为

$$S_{\mathrm{vernier}}=M_1S_{\mathrm{PDMS}}+M_2S_{\mathrm{air}},\tag{6}$$

式中：M_1为将空气腔作为参考腔，级联双腔灵敏度相对于单个PDMS腔的放大倍率；M_2为将PDMS腔作为参考腔，级联双腔灵敏度相对于单个空气腔的放大倍率。M_1和M_2可分别表示为

$$\begin{cases}M_1=\dfrac{R_2}{R_2-R_1}=\dfrac{n_1L_1}{n_1L_1-n_2L_2}\\ M_2=\dfrac{R_1}{R_1-R_2}=\dfrac{n_2L_2}{n_2L_2-n_1L_1}\end{cases}。\tag{7}$$

对该传感器的温度传感特性进行了仿真分析，仿真参数分别为：L_1=165.0 μm，L_2=270.0 μm；n_1=1.41，n_2=1.0；$\alpha=9.6\times10^{-4}$/℃，$\beta=-5\times10^{-4}$/℃；d=1.0 mm，λ_{s}=1550 nm；$I_1=5\times10^{-4}$，$I_2=1\times10^{-3}$，$I_3=1\times10^{-4}$。级联前后PDMS腔和空气腔的干涉谱仿真结果如图2所示，单个PDMS和单个空气腔的FSR分别为5.20 nm和4.40 nm，双腔级联后呈现明显的包络现象，干涉谱包络的自由范围为32.20 nm。由式（7）计算可知，M_1=5.5，M_2=6.5。图3为外界温度分别为40.0 ℃和41.0 ℃时，单个PDMS腔、单个空气腔以及级联双腔的干涉谱。由图3可知，当温度由40.0 ℃升高至41.0 ℃时，单个PDMS腔的干涉谱红移0.9 nm，单个空气腔的干涉谱蓝移2.6 nm，级联双腔干涉谱包络蓝移24.8 nm。相对于单个PDMS腔，该级联双腔灵敏度提高了27.6倍；相对于单个空气腔，该级联双腔灵敏度提高了9.5倍。

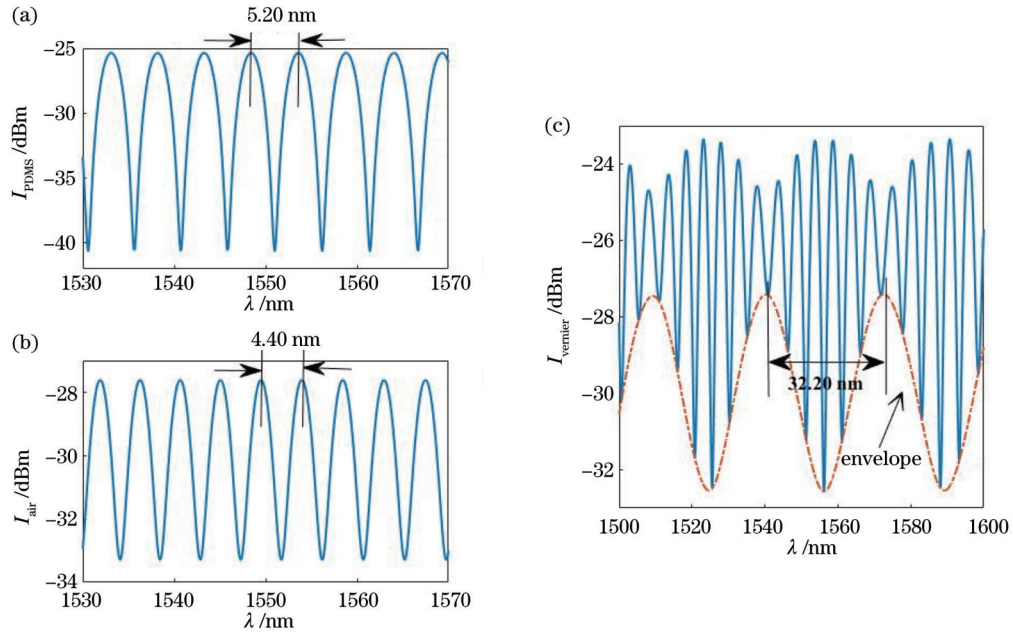

图 2　级联前后 PDMS 腔和空气腔的干涉谱仿真结果。(a) 单个 PDMS 腔干涉谱；(b) 单个空气腔干涉谱；(c) 级联双腔干涉谱

Fig. 2　Simulation results of interference spectra of PDMS cavity and air cavity before and after cascading. (a) Interference spectrum of single PDMS cavity; (b) interference spectrum of single air cavity; (c) interference spectrum of cascaded two cavities

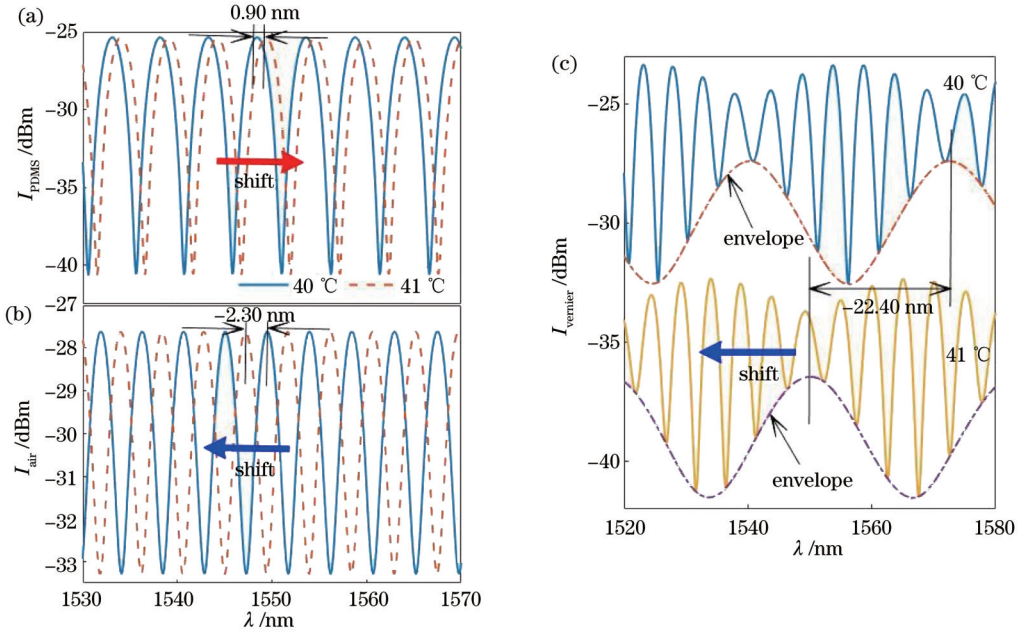

图 3　温度由 40 ℃上升到 41 ℃时干涉谱的变化。(a) 单个 PDMS 腔；(b) 单个空气腔；(c) 级联双腔

Fig. 3　Interference spectrum shift with temperature increasing from 40 ℃ to 41 ℃. (a) Single PDMS cavity; (b) single air cavity; (c) cascaded two cavities

3　实验结果及分析

图 4 为本文实验制备的 PDMS 腔显微图，制备过程如下：1)将端面切割平整的 SMF(直径约为 125 μm)与 HCF(内径约为 75 μm，外径约为 150 μm)对芯熔接；2)在显微镜下，将 HCF 切割为所需长度，然后将 SMF-HCF 固定在玻璃片上；3)将道康宁硅胶 Sylgard 184-A 和 Sylgard 184-B 按质量 10∶1 的比例混合搅拌均匀，使其成为液态 PDMS；4)使用吸管将液态 PDMS 滴在 SMF-HCF 上，利用毛细现象使液态 PDMS 逐渐充满 HCF；5)使用酒精棉擦去 HCF 外多余的 PDMS，并将其放置在 80 ℃的温控箱内 1 h，使液态 PDMS 固化，从而形成所需的 PDMS 腔。不同温度下，PDMS 腔的干涉谱如图 5 所示，1550 nm 附近 PDMS 腔的干涉谱 FSR 为 6.0 nm，利用 FSR 与腔长的关系，可知 PDMS 腔的腔长为 142.0 μm。随着温度

的升高，PDMS的干涉谱逐渐向长波方向移动，即红移，该实验结果与理论分析结果[见式(3)]相符。红移的原因是：当温度增加时，PDMS腔的腔长变化起到了主要作用，腔长变化引起的PDMS腔相位增加大于折射率变化引起的相位减小。在40～60 ℃的温度变化范围内，PDMS腔的温度灵敏度为0.56 nm/℃，该实验结果明显低于仿真结果0.9 nm/℃，原因在于PDMS腔内的PDMS不是自由膨胀，受HCF内壁拉力的限制。

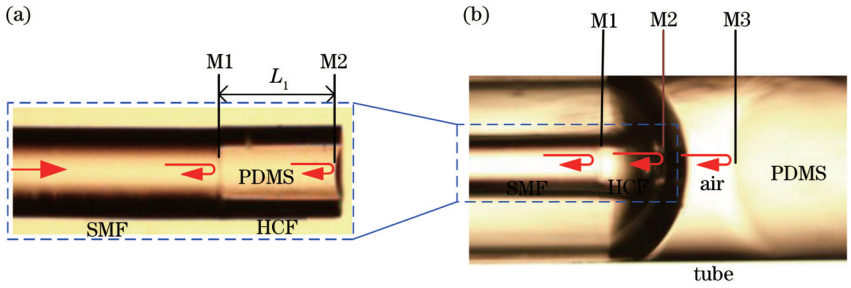

图4　PDMS腔显微图。(a) 封装前PDMS腔的显微图；(b) 封装后PDMS腔和空气腔显微图

Fig. 4　Micrograph of PDMS cavity. (a) Micrograph of PDMS cavity before packaging; (b) micrograph of PDMS cavity and air cavity after packaging

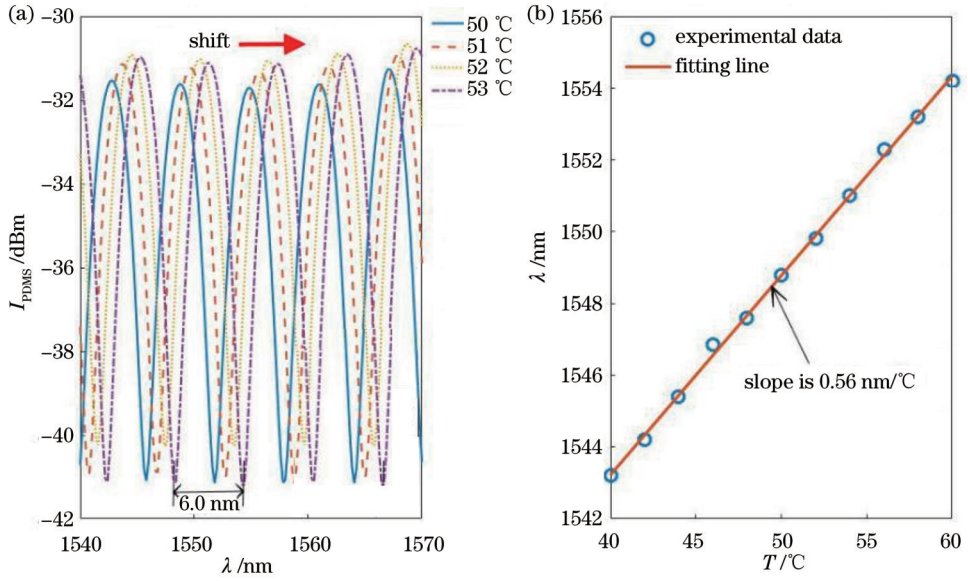

图5　不同温度下PDMS腔的干涉谱及PDMS腔峰值波长随温度的变化。(a) PDMS腔的干涉谱；(b) PDMS腔干涉谱峰值波长随温度变化曲线

Fig. 5　Interference spectra of PDMS cavity under different temperatures and peak wavelength of PDMS cavity versus temperature. (a) Interference spectra of PDMS cavity; (b) curve of peak wavelength of interference spectra of PDMS cavity versus temperature

将前面制备好的SMF-HCF封装在一端注入PDMS(PDMS长度约为1.0 mm)的石英管(内径约为250 μm，外径约为360 μm)内，且两PDMS间形成空气腔，如图1(b)所示。通过精确控制空气腔的长度，使其与PDMS腔近似相等时，此时双腔将产生游标效应，干涉谱呈包络现象。本文搭建的实验系统如图6所示，该实验系统由放大自发辐射(ASE)光源(C+L波段)、光谱仪(型号为AQ6370C，分辨率为0.02 nm)、光纤耦合器、级联双腔传感器和温控箱(型号为ZKXFB-1，分辨率为0.1 ℃)构成。ASE光源发出的信号光经光纤耦合器后被级联双腔传感器反射，反射后的干涉信号经耦合器后被光谱仪接收。室温(20 ℃)下，级联双腔传感器的干涉谱如图7所示，可以看出，级联双腔干涉谱呈明显的包络现象，干涉谱包络的FSR为32.9 nm。实验研究了级联双腔的温度传感特性，图8为不同温度下级联双腔的干涉谱包络，随温度逐渐升高，干涉谱包络逐渐向短波方向移动，即蓝移。两个干涉仪游标效应产生的干涉谱包络是红移还是蓝移受两个因素的影响：一是两个干涉仪FSR的相对大小；二是两个干涉仪干涉谱的相对移动方向。具体结论如下：1)当干涉仪2的FSR小于干涉仪1时，如果干涉仪2相对于干涉仪1红移，则两干涉仪产生的干涉谱包络红移，反之则蓝移；2)当干涉仪2的FSR大于干涉仪1时，如果干涉仪2相对于干涉仪1红移，则两干涉仪产生的干涉谱包络蓝移，反之则红移。对于该传感器，当温度升高时，受PDMS膨胀挤压的影响，空

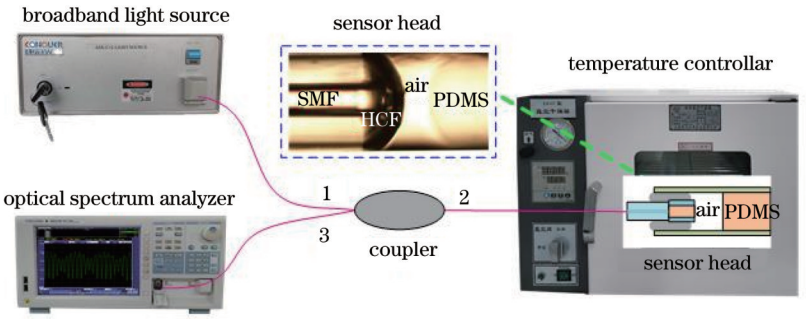

图 6　温度传感器装置图

Fig. 6　Temperature sensor device diagram

气腔腔长减小，其干涉谱蓝移，同时由于 PDMS 腔的干涉谱红移，因此，PDMS 腔的干涉谱相对于空气腔红移。结合干涉谱包络的蓝移的实验结果，可以推断出 PDMS 腔的 FSR 大于空气腔。将 R_{en}=32.9 nm 和 R_{PDMS}=6.0 nm 代入公式 $R_{en}=R_{air}*R_{PDMS}/(R_{PDMS}-R_{air})$ 计算可得 $R_{air}\approx$5.1 nm，进一步，由公式 $R_{air}=\lambda^2/2n_2L_2$ 计算可知 $L_2\approx$235.5 μm。

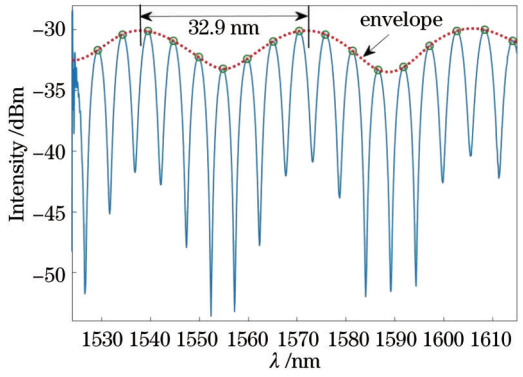

图 7　级联双腔干涉谱

Fig. 7　Interference spectrum of cascaded two cavities

为了研究该传感器测量结果的稳定性和重复性，将其放入温控箱内，做了该传感器的升降温实验。由 40 ℃逐渐升高到 42 ℃，然后逐渐下降到 40 ℃，反复 2 次。在升降温过程中，每间隔 0.2 ℃记录 1 次干涉谱包络峰值波长，然后，将所得各组升温和降温数据进行线性拟合，得到的干涉谱包络峰值波长随温度的变化曲线如图 9 所示。结果表明：2 次升降温过程中该传感器

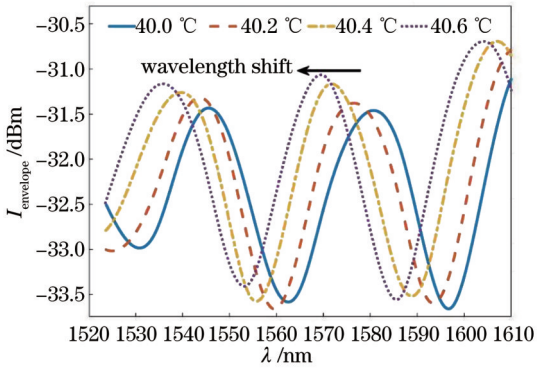

图 8　不同温度下干涉谱包络

Fig. 8　Interference spectral envelopes under different temperatures

的灵敏度分别为 −21.10、−20.25、−20.88、−19.96 nm/℃，其平均值约为 −20.55 nm/℃，约为单个 PDMS 腔（灵敏度为 0.56 nm/℃）的 37 倍；对于 2 次升降温过程，该传感器灵敏度的最大误差约为 5%，误差产生的原因主要是温控箱的分辨率偏低造成的。此外，实验获得的该传感器的灵敏度略低于仿真结果（−24.8 nm/℃），原因在于，空气腔两侧的 PDMS 均非自由膨胀，实际膨胀系数小于仿真值。

表 1 对几种基于游标效应的光纤温度传感器的性能进行了对比分析，结果表明：只有基于 Sagnac 干涉仪级联的光纤传感器[26]的灵敏度高于本文提出的传感器，该传感器的长度约为 2.1 m，远大于本文提出的传感器（约 1 mm）；本文提出的传感器的温度灵敏度高于

表 1　不同光纤传感器的温度性能比较

Table 1　Comparison of temperature sensitivities of different fiber sensors

Sensor configuration	Range /℃	Sensitivity /(nm·℃$^{-1}$)	Size /μm	Reference
Parallel air and PDMS FPIs	46-50	17.758	~140	[22]
Cascaded air and PDMS FPIs	40-56	3.980	~600	[23]
Two parallel PDMS FPIs	50-60	−14.600	~200	[24]
Parallel two SIs	31-35	78.984	~2100000	[26]
Two cascaded all-fiber FPIs	250-1050	1.109	~8000	[27]
Using an air-cavity with PDMS at both ends	40-42	−21.100	~1000	This work

表中所有基于PDMS填充的FPI传感器[22-24]；受PDMS熔点较低的限制，所有基于PDMS填充的温度传感器的测量范围远低于全光纤传感器[27]。综上所述，本文提出的温度传感器具有结构紧凑、灵敏度高的优点，其温度测量范围依赖于PDMS的温度特性。

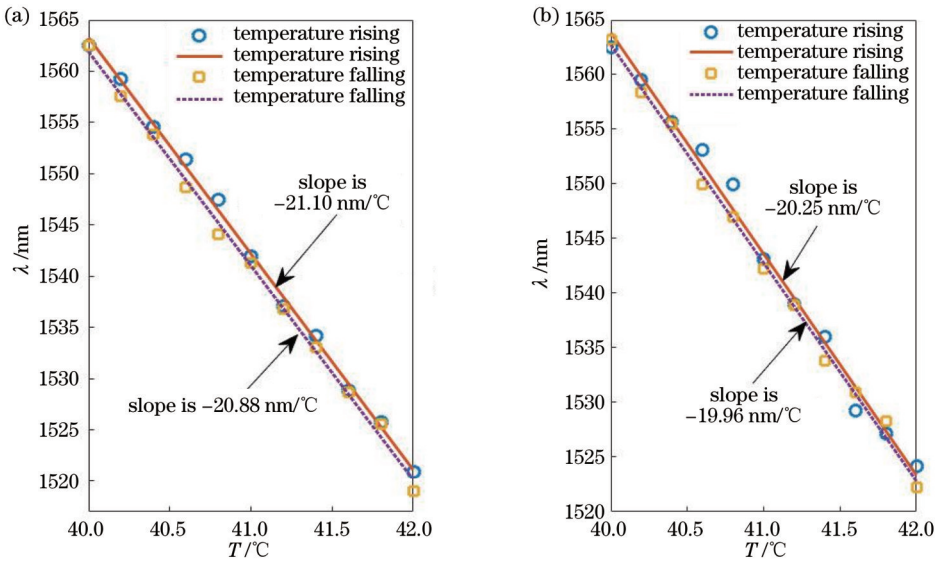

图9　升降温过程中干涉谱包络峰值随温度的变化曲线

Fig. 9　Peak wavelength shift of interference spectral envelope with temperature rising and falling

4　结　　论

提出并制备了一种SMF-PDMS-air-PDMS光纤温度传感器，利用PDMS腔和空气腔产生游标效应，通过双侧PDMS的热膨胀实现温度增敏。实验结果表明，该光纤温度传感器的干涉谱呈现出明显的包络现象，在40～42 ℃范围内，随着温度的增加，干涉谱包络逐渐蓝移，其温度灵敏度约为−20.55 nm/℃，约为单个PDMS腔的37倍。该传感器具有灵敏度高、稳定性好、结构紧凑、成本低廉等优点，在工业过程控制、健康监测、生物化学反应控制等领域具有重要的应用价值。

参　考　文　献

[1] 范维文，万洪丹，陈彧芳，等. 基于二模-单模微纳光纤Sagnac环的高灵敏度光纤温度传感器[J]. 光学学报，2022，42(16)：1606001.
Fan W W，Wan H D，Chen Y F，et al. Highly sensitive fiber optic temperature sensor based on two-mode-single-mode microfiber Sagnac loop[J]. Acta Optica Sinica，2022，42(16)：1606001.

[2] 刘福禄，张钰民，庄炜，等. 基于游标效应和基底增敏的复合光纤结构温度传感器[J]. 光学学报，2021，41(15)：1506002.
Liu F L，Zhang Y M，Zhuang W，et al. Fiber temperature sensor with composite structure based on vernier effect and substrate sensitization[J]. Acta Optica Sinica，2021，41(15)：1506002.

[3] 胡白燕，文富荣，程永山，等. 基于级联腔法布里-珀罗干涉仪的温度和压力同时测量[J]. 激光与光电子学进展，2021，58(19)：1906006.
Hu B Y，Wen F R，Cheng Y S，et al. Simultaneous measurement of temperature and pressure based on cascaded Fabry-Pérot interferometer[J]. Laser & Optoelectronics Progress，2021，58(19)：1906006.

[4] 郭海若，刘琨，江俊峰，等. 基于可调谐激光器的光纤高低温力热复合多参量传感系统[J]. 中国激光，2021，48(19)：1906003.
Guo H R，Liu K，Jiang J F，et al. Optical fiber high and low temperature mechanical and thermal multi-parameter sensing system based on tunable laser[J]. Chinese Journal of Lasers，2021，48(19)：1906003.

[5] 王东平，王伟，张军英，等. 光纤法布里-珀罗传感器双峰-干涉级次定位联合解调算法[J]. 光学学报，2022，42(16)：162001.
Wang D P，Wang W，Zhang J Y，et al. Peak-to-peak and interference-order positioning joint demodulation algorithm for fiber-optic Fabry-Pérot sensors[J]. Acta Optica Sinica，2022，42(16)：162001.

[6] 刘燕燕，刘磊，刘雪强，等. 基于Vernier效应的法布里-珀罗传感器增敏方法[J]. 光学学报，2019，39(4)：0428001.
Liu Y Y，Liu L，Liu X Q，et al. Sensitivity improvement of Fabry-Pérot sensor based on vernier effect[J]. Acta Optica Sinica，2019，39(4)：0428001.

[7] Liu G G，Han M，Hou W L. High-resolution and fast-response fiber-optic temperature sensor using silicon Fabry-Pérot cavity[J]. Optics Express，2015，23(6)：7237-7247.

[8] Hernández-Romano I，Cruz-Garcia M A，Moreno-Hernández C，et al. Optical fiber temperature sensor based on a microcavity with polymer overlay[J]. Optics Express，2016，24(5)：5654-5661.

[9] Chen M Q，Zhao Y，Xia F，et al. High sensitivity temperature sensor based on fiber air-microbubble Fabry-Pérot interferometer with PDMS-filled hollow-core fiber[J]. Sensors and Actuators A：Physical，2018，275：60-66.

[10] He C Y，Fang J B，Zhang Y N，et al. High performance all-fiber temperature sensor based on coreless side-polished fiber wrapped with polydimethylsiloxane[J]. Optics Express，2018，26(8)：9686-9699.

[11] 徐廷廷，杨玉强，杨文龙，等. 基于PDMS膜封装空芯光纤的级联双腔温度传感器[J]. 光学学报，2022，42(8)：0806004.
Xu T T，Yang Y Q，Yang W L，et al. Cascaded double-cavity temperature sensor based on hollow fibers encapsulated by

PDMS membrane[J]. Acta Optica Sinica, 2022, 42(8): 0806004.
[12] 古洪, 罗彬彬, 石胜辉, 等. 基于极大倾角光纤光栅Sagnac游标干涉仪的折射率传感器[J]. 光学学报, 2022, 42(20): 2006004.
Gu H, Luo B B, Shi S H, et al. Refractive index sensor based on excessively tilted fiber grating Sagnac vernier interferometer [J]. Acta Optica Sinica, 2022, 42(20): 2006004.
[13] 方莎莎, 吴许强, 张刚, 等. 基于游标效应的高灵敏光纤温度和应变传感器[J]. 中国激光, 2021, 48(1): 0106004.
Fang S S, Wu X Q, Zhang G, et al. High-sensitivity fiber optic temperature and strain sensors based on the vernier effect[J]. Chinese Journal of Lasers, 2021, 48(1): 0106004.
[14] 蔡礼邹, 覃亚丽, 蔡小磊, 等. 基于游标原理的法布里-珀罗温度传感器的增敏方法[J]. 激光与光电子学进展, 2021, 58(11): 1106004.
Cai L Z, Qin Y L, Cai X L, et al. Sensitization method of Fabry-Pérot temperature sensor based on vernier principle[J]. Laser & Optoelectronics Progress, 2021, 58(11): 1106004.
[15] 黄炳森, 高社成, 黄新成, 等. 高敏光纤法布里-珀罗干涉应变传感器[J]. 光学学报, 2020, 40(6): 0606002.
Huang B S, Gao S C, Huang X C, et al. High-sensitivity fiber Fabry-Pérot interferometer strain sensor[J]. Acta Optica Sinica, 2020, 40(6): 0606002.
[16] Dai X S, Wang S, Jiang J F, et al. High-sensitive MEMS Fabry-Pérot pressure sensor employing an internal-external cavity Vernier effect[J]. Optics Express, 2022, 30(18): 31840-31851.
[17] Lang C P, Liu Y, Liao Y Y, et al. Ultra-sensitive fiber-optic temperature sensor consisting of cascaded liquid-air cavities based on vernier effect[J]. IEEE Sensors Journal, 2020, 20(10): 5286-5291.
[18] Liao H, Lu P, Fu X, et al. Sensitivity amplification of fiber-optic in-line Mach-Zehnder Interferometer sensors with modified Vernier-effect[J]. Optics Express, 2017, 25(22): 26898-26909.
[19] Shao L Y, Luo Y, Zhang Z Y, et al. Sensitivity-enhanced temperature sensor with cascaded fiber optic Sagnac interferometers based on Vernier-effect[J]. Optics Communications, 2015, 336: 73-76.
[20] Yang Y Q, Wang Y G, Zhao Y X, et al. Sensitivity-enhanced temperature sensor by hybrid cascaded configuration of a Sagnac loop and a F-P cavity[J]. Optics Express, 2017, 25(26): 33290-33296.
[21] Li J W, Zhang M, Wan M G, et al. Ultrasensitive refractive index sensor based on enhanced Vernier effect through cascaded fiber core-offset pairs[J]. Optics Express, 2020, 28(3): 4145-4155.
[22] Hou L Y, Zhao Ch L, Xu B, et al. Highly sensitive PDMS-filled Fabry-Pérot interferometer temperature sensor based on the Vernier effect[J]. Applied Optics, 2019, 58(18): 4858-4865.
[23] Fu X H, Ran R, Li Q N, et al. A few mode fiber temperature sensor filled with PDMS based on vernier effect[J]. IEEE Photonics Journal, 2021, 13(5): 6800205.
[24] Mu X G, Gao J L, Yang Y Q, et al. Parallel polydimethylsiloxane-cavity Fabry-Pérot interferometric temperature sensor based on enhanced vernier effect[J]. IEEE Sensors Journal, 2022, 22(2): 1333-1337.
[25] Quan M R, Tian J J, Yao Y. Ultra-high sensitivity Fabry-Pérot interferometer gas refractive index fiber sensor based on photonic crystal fiber and Vernier effect[J]. Optics Letters, 2015, 40(21): 4891-4894.
[26] Zhao Y F, Dai M L, Chen Z M, et al. Ultrasensitive temperature sensor with Vernier-effect improved fiber Michelson interferometer[J]. Optics Express, 2021, 29(2): 1090-1101.
[27] Zhang P, Tang M, Gao F, et al. Simplified hollow-core fiber-based Fabry-Pérot interferometer with modified vernier effect for highly sensitive high-temperature measurement[J]. IEEE Photonics Journal, 2015, 7(1): 7100210.

Cascaded Double-Cavity Temperature Sensor Sensitized by Polydimethylsiloxane

Yang Yuqiang[1,2,4], Gao Jiale[1,4], Mu Xiaoguang[3*], Wang Ji[2,4**], Yang Wenhu[1,4], Li Yitong[2,4], Wang Chuhong[4]

[1]*Shenzhen Institute of Guangdong Ocean University, Shenzhen* 518120, *Guangdong, China*;
[2]*Guangdong Provincial Engineering Research Center for Ship Intelligence and Safety, Guangdong Ocean University, Zhanjiang* 524088, *Guangdong, China*;
[3]*College of Mechanical Engineering, Guangdong Ocean University, Zhanjiang* 524088, *Guangdong, China*;
[4]*Research Center of Guangdong Smart Oceans Sensor Networks and Equipment Engineering, Guangdong Ocean University, Zhanjiang* 524088, *Guangdong, China*

Abstract

Objective Temperature is the most basic and important physical quantity in scientific research and industrial production, so temperature measurement with high sensitivity is essential. Due to the advantages of corrosion resistance, high safety, electromagnetic interference resistance, small size, compact structure, and easy integration, the fiber optic Fabry-Pérot interferometer (FPI) sensor has widely drawn the attention of global scholars. However, the sensitivity of the all-fiber FPI temperature sensor is only 84.6 pm/℃ due to the low thermal expansion and thermal-optical coefficient of the quartz fiber. There are two effective ways to increase the sensitivity of FPIs. One is to use polydimethylsiloxane (PDMS) which has a high coefficient of thermal expansion, and the other is to generate vernier effect. The effective combination of PDMS and vernier effect will further improve the sensitivity of FPIs. In this study, a temperature sensor based on PDMS and vernier

effect is proposed and fabricated. With the help of PDMS expansion and vernier effect, the sensor has excellent temperature characteristics.

Methods In this study, a cascaded double-cavity temperature sensor based on PDMS sensitization is proposed, which is composed of a PDMS cavity and an air cavity in cascade (Fig. 1). The PDMS cavity is formed by filling PDMS into a section of hollow core fiber with one end fused with the single mode fiber (SMF). The air cavity is formed by filling the PDMS cavity into a tube with a section of PDMS. The optical paths of PDMS cavity and air cavity are close but not equal, so the vernier effect is generated, and an envelope appears in the spectrum. The two cavities have opposite temperature responses, so the sensitivity of the sensor can be greatly improved by vernier effect. When the temperature increases, the length of the air cavity changes greatly due to the expansion of the PDMS at both ends, which greatly improves the temperature response of the air cavity and results in a further increase in the sensitivity of the sensor. Under the dual action of PDMS and vernier effect, the sensor has excellent temperature characteristics.

Results and Discussions The temperature performance of the sensor are theoretically analyzed and simulated. In the simulation, the free spectral ranges (FSRs) of PDMS cavity and air cavity are 5.20 nm and 4.40 nm, respectively, and the obtained spectrum envelope of the cascaded structure is 32.20 nm (Fig. 2). When the temperature rises from 40 to 41 ℃, the PDMS cavity has a red shift of 0.9 nm, and the air cavity has a blue shift of 2.6 nm, while the spectral envelope has a blue shift of 24.8 nm, which is 27.6 times as much as that of single PDMS cavity and 9.5 times as much as that of the single air cavity. In the experiment, the sensor is put into a temperature control box, and its interference spectrum is measured by an optical spectrum analyzer (Fig. 6). There is an obvious envelope with the FSR of 32.9 nm in the interference spectrum of the sensor (Fig. 7), which shows that vernier effect is generated. When the temperature increases, the spectral envelope shifts gradually to a short wavelength (Fig. 7). The temperature rising and falling experiments are carried out to investigate the stability and repeatability of the sensor, and the peak wavelength of the envelope is recorded at every interval of 0.2 ℃. By linearly fitting the data of wavelength shift versus temperature in the range from 40 to 42 ℃, the sensitivities of −21.10, −20.25, −20.88, and −19.96 nm/℃ are obtained (Fig. 9), and the average sensitivity is calculated to be about −20.55 nm/℃, which is 37 times as much as that of a single PDMS cavity (0.56 nm/℃). The maximum error between the sensitivities is about 5%, and the error is mainly caused by the low resolution of the temperature control box. In addition, the sensitivity of the sensor is slightly lower than the simulation results (−24.8 nm/℃). The reason is that the PDMS in the sensor is not freely expanded, and its actual expansion is smaller than that in ideal conditions. Compared with other FPI sensors based on PDMS, the proposed sensor has the highest temperature sensitivity (Table 1).

Conclusions A cascaded double-cavity temperature sensor based on PDMS sensitization is proposed and prepared, which is composed of a PDMS cavity and an air cavity. The optical paths of the two cavities are similar but not equal, and the two cavities have opposite temperature responses, so the enhanced vernier effect is generated, and an envelope appears in the interference spectrum. In addition, the sensitivity of the sensor is further improved by the expansion of the PDMS at both ends of the air cavity. Under the dual effect of PDMS and enhanced vernier effect, the sensor has an ultra-high temperature sensitivity. The experimental results show that the temperature sensitivity of the sensor is about −20.55 nm/℃ in the range of 40-42 ℃, which is about 37 times as much as that of the single PDMS cavity. With the help of PDMS and vernier effect, the sensor has excellent temperature characteristics. Due to the advantages of electromagnetic immunity, compact structure, high sensitivity, excellent stability, and easy integration, the sensor is promising for applications in scientific research and industrial production.

Key words fiber optics and optical communication; optical fiber sensor; Fabry-Pérot interferometer; vernier effect; polydimethylsiloxane